The Role of Substorm Injections on the Extreme Geo-Effectiveness Observed in the Inner Magnetosphere on the 8 September 2017 Geomagnetic Storm

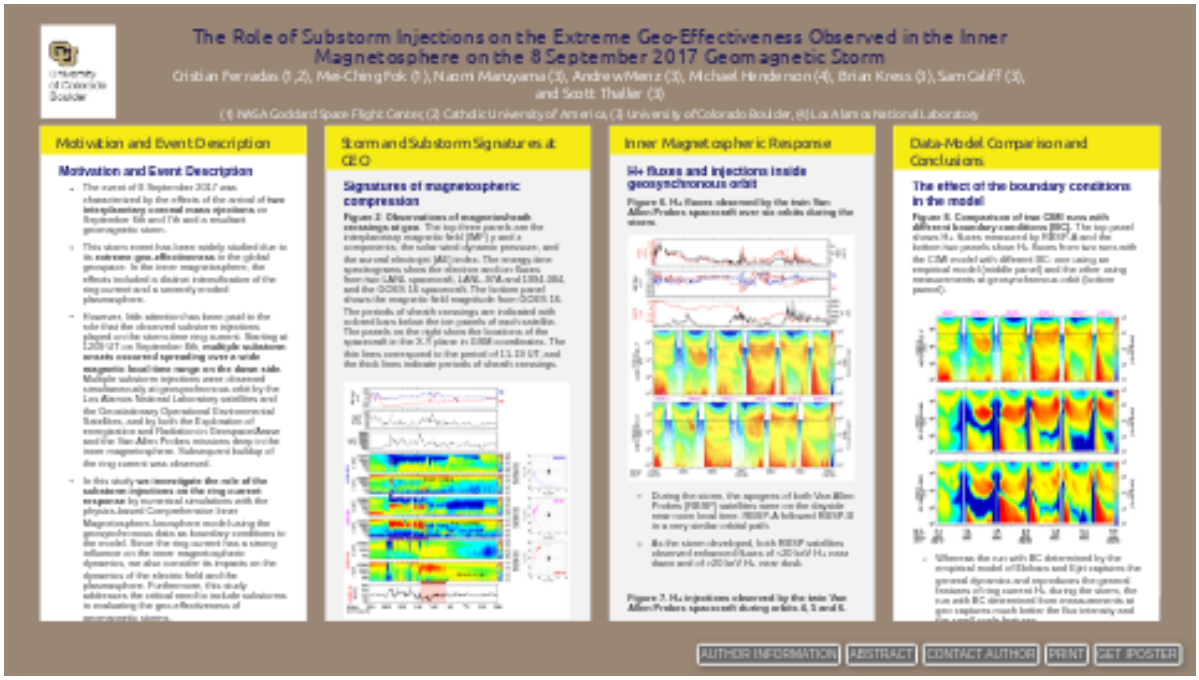

Cristian Ferradas (1,2), Mei-Ching Fok (1), Naomi Maruyama (3), Andrew Menz (3), Michael Henderson (4), Brian Kress (3), Sam Califf (3), and Scott Thaller (3)

(1) NASA Goddard Space Flight Center, (2) Catholic University of America, (3) University of Colorado Boulder, (4) Los Alamos National Laboratory

PRESENTED AT:

AGU FALL MEETING
Online Everywhere | 1–17 December 2020

MOTIVATION AND EVENT DESCRIPTION

Motivation and Event Description

- The event of 8 September 2017 was characterized by the effects of the arrival of **two interplanetary coronal mass ejections** on September 6th and 7th and a resultant geomagnetic storm.

- This storm event has been widely studied due to its **extreme geo-effectiveness** in the global geospace. In the inner magnetosphere, the effects included a distinct intensification of the ring current and a severely eroded plasmasphere.

- However, little attention has been paid to the role that the observed substorm injections played on the storm-time ring current. Starting at 1209 UT on September 8th, **multiple substorm onsets occurred spreading over a wide range of magnetic local times on the dawn side**. Multiple substorm injections were observed simultaneously at geosynchronous orbit by the Los Alamos National Laboratory satellites and the Geostationary Operational Environmental Satellites, and by both the Exploration of energization and Radiation in Geospace/Arase and the Van Allen Probes missions deep in the inner magnetosphere. Subsequent buildup of the ring current was observed.

- In this study **we investigate the role of the substorm injections on the ring current response** by numerical simulations with the physics-based Comprehensive Inner Magnetosphere-Ionosphere model using the geosynchronous data as boundary conditions to the model. Since the ring current has a strong influence on the inner magnetospheric dynamics, we also consider its impacts on the dynamics of the electric field and the plasmasphere. Furthermore, this study addresses the critical need to include substorms in evaluating the geo-effectiveness of geomagnetic storms.

Solar Wind Drivers

Figure 1. Solar wind parameters and geomagnetic indices during the geomagnetic storm. The arrival of two interplanetary coronal mass ejections (ICMEs) were observed late Septermber 6 and late September 7. During the development of the storm on September 8, two dips in the Dst index profile are observed.

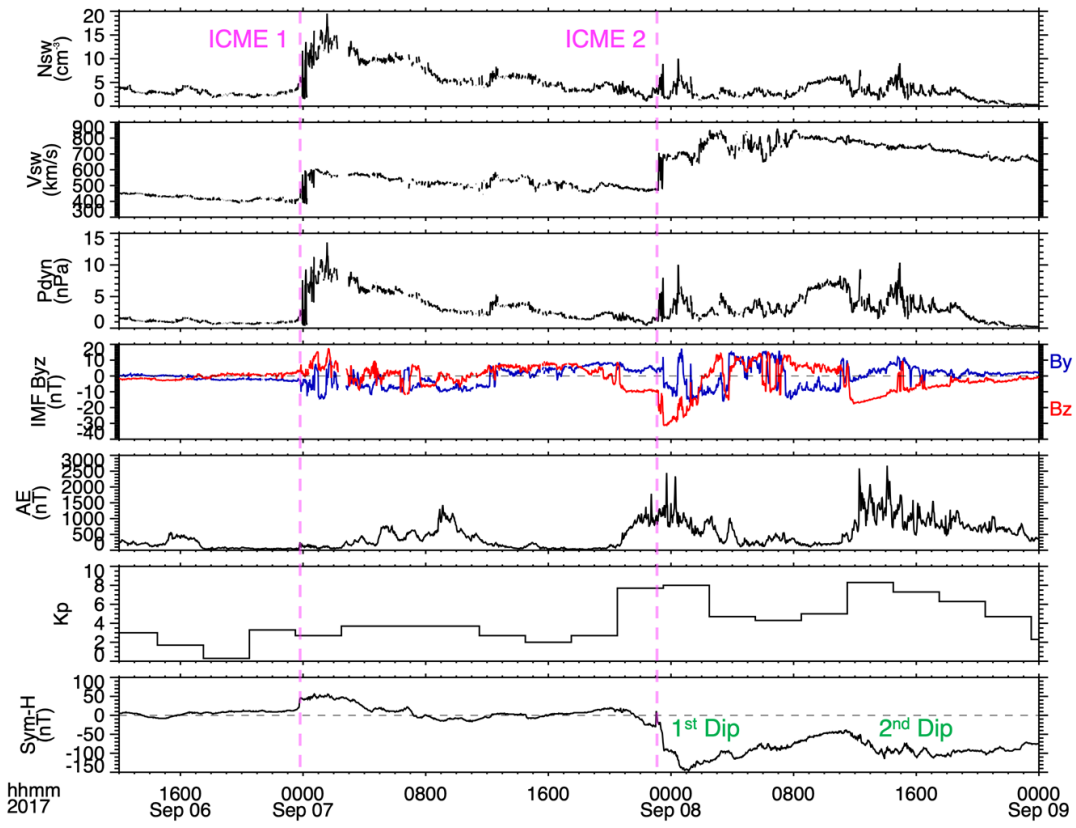

STORM AND SUBSTORM SIGNATURES AT GEO

Signatures of magnetospheric compression

Figure 2. **Observations of magnetosheath crossings at geo during the period of 1100-1900 UT on September 8**. The top three panels are the interplanetary magnetic field (IMF) y and z components, the solar wind dynamic pressure, and the auroral electrojet (AE) index. The energy-time spectrograms show the electron and ion fluxes from two LANL spacecraft, LANL-97A and 1994-084, and the GOES 16 spacecraft. The bottom panel shows the magnetic field magnitude from GOES 16. The periods of sheath crossings are indicated with colored bars below the ion panels of each satellite. The panels on the right show the locations of the spacecraft in the X-Y plane in GSM coordinates. The thin lines correspond to the period of 11-19 UT, and the thick lines indicate periods of sheath crossings.

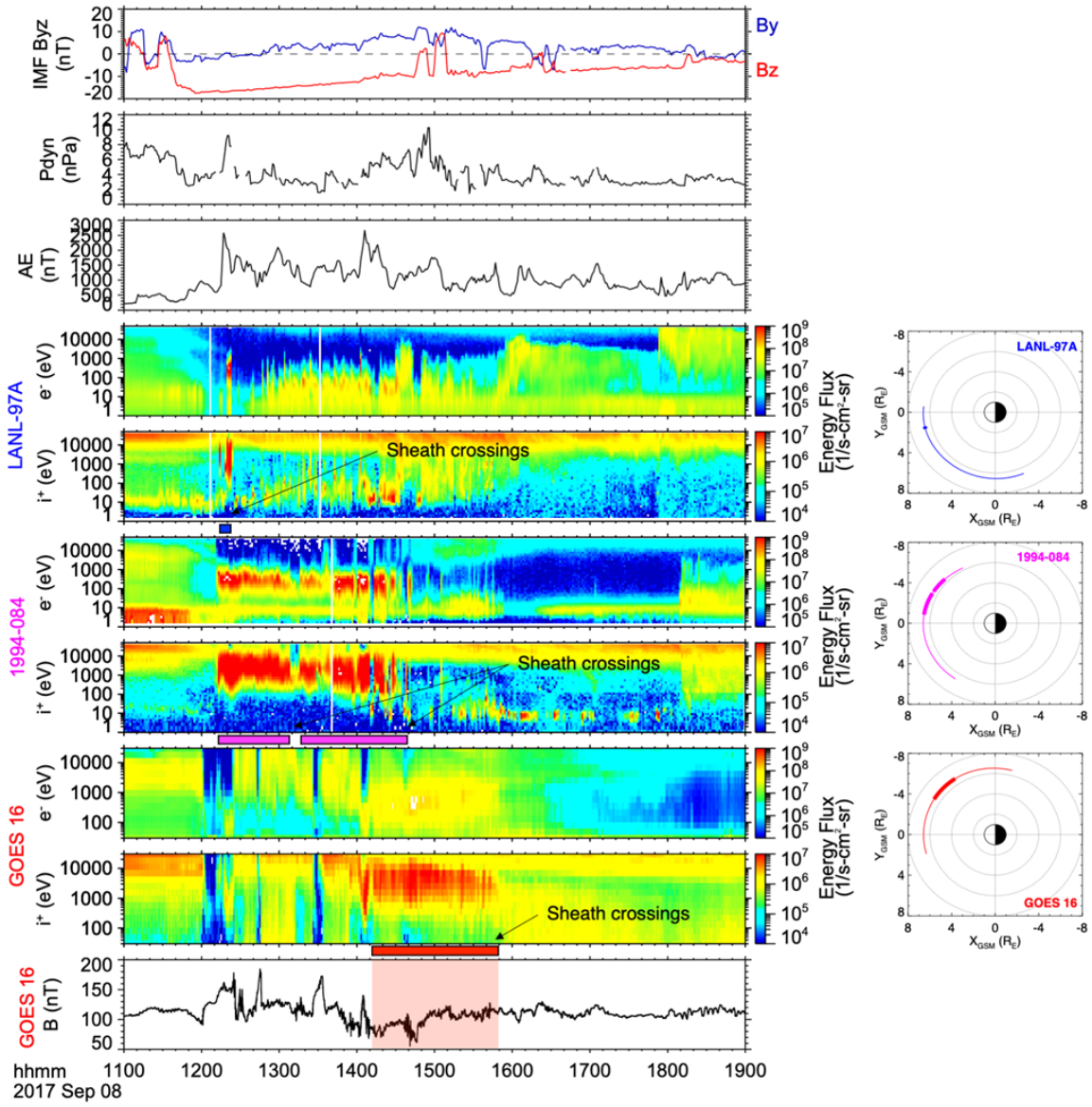

- At ~1220 UT, during a period of magnetopause erosion (strong negative IMF Bz) two spacecraft on the dayside encountered the magnetosheath due to compression of the magnetosphere (peak in solar wind pressure).
- At this time, LANL-97A was in the afternoon sector and observed the sheath for a brief period (~10 min), whereas 1994-084, located in the pre-noon sector, observed the sheath intermittently over a period of over two hours.
- At ~1410 UT GOES 16 was at MLT~08 and also crossed the magnetosheath and continued to do so intermittently for over 1.5 hours. During most of this period, 1994-084 was in the afternoon sector and did not cross the magnetosheath.

- This suggests that the magnetosphere was compressed asymmetrically in the dawn-dusk direction, being compressed more strongly and over a prolonged period on the dawnside.

Figure 3. **Observations of lobe encounters at geo during the period of 1100-1900 UT on September 8**. Similar format to Figure 2, except that the energy-time spectrograms show the electron and ion fluxes from LANL-04A, LANL-01A and GOES 16. The periods of lobe encounters are indicated with colored bars below the ion panels of each satellite. The panels on the right show the locations of the spacecraft in the X-Y plane in GSM coordinates. The thin lines correspond to the period of 11-19 UT, and the thick lines indicate periods of lobe encounters.

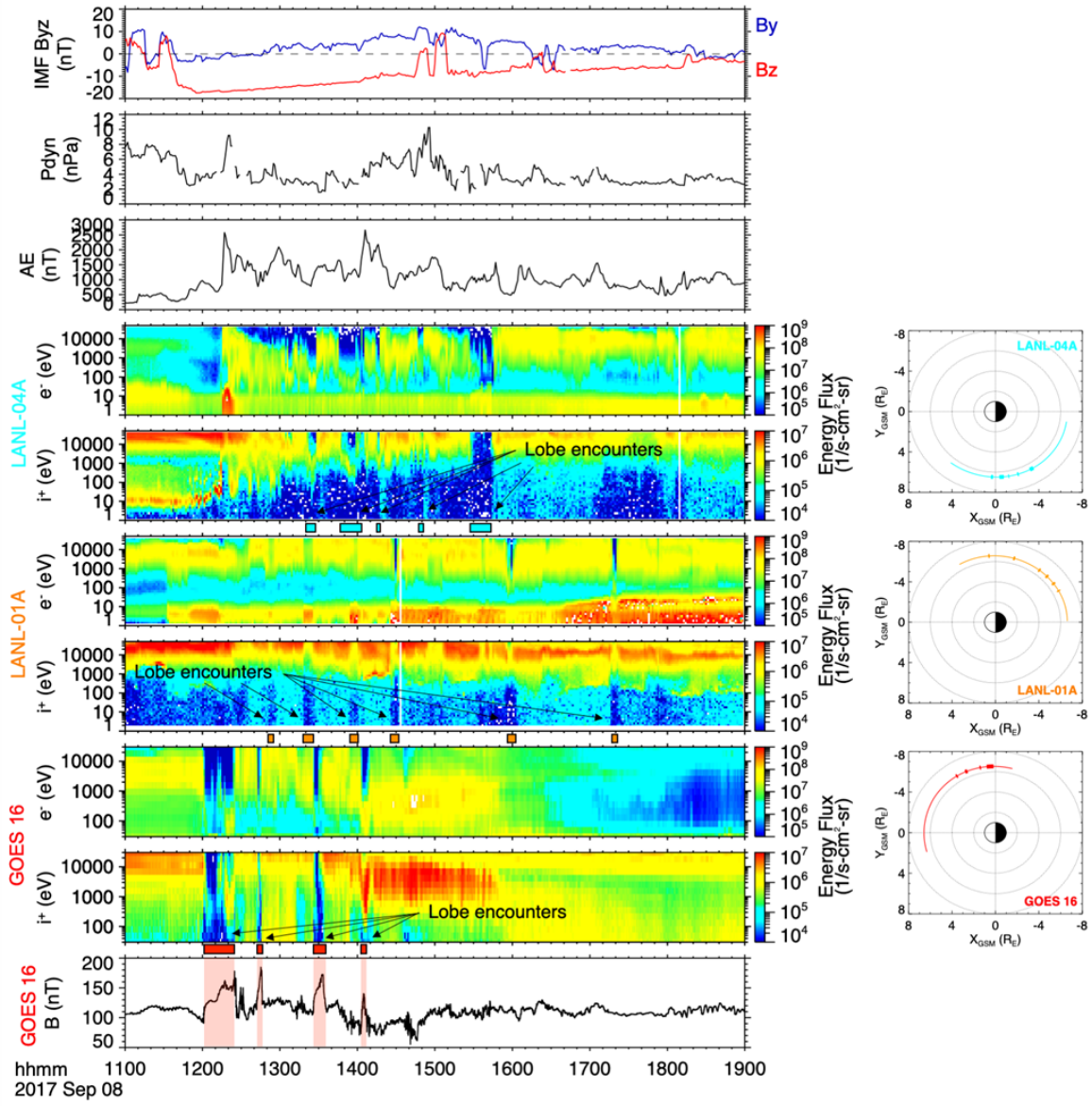

- Starting at ~1200, 1250, and 1320 UT, GOES 16, LANL-01A, and LANL-04A exhibit intermitent intervals when the spacecraft were apparently on open field lines of the magnetospheric lobe. Some of these periods are interpreted as lobe encounters or near-lobe encounters.
- These intermitent intervals were observed over periods of ~2, ~4, and ~2 hours, for each of the spacecraft respectively.
- These encounters were observed both on the dawnside and the duskside.
- Lobe encounters by geosynchronous satellites are rare (Thomsen et al. 1994). Moreover, a statistical survey of geosynchronous lobe encounters showed that they are primarily dawnside phenomena.
- Therefore, these observations suggest that the magnetic field was severly and uncommonly distorted during this storm.

Signatures of particle injections

Figure 4. **Observations of particle injections at geo**. Similar format to Figure 2, but showing the timing (vertical dashed lines) and the location (panels on the right) of particle injections observed by LANL-01A, GOES 16 and 1994-084.

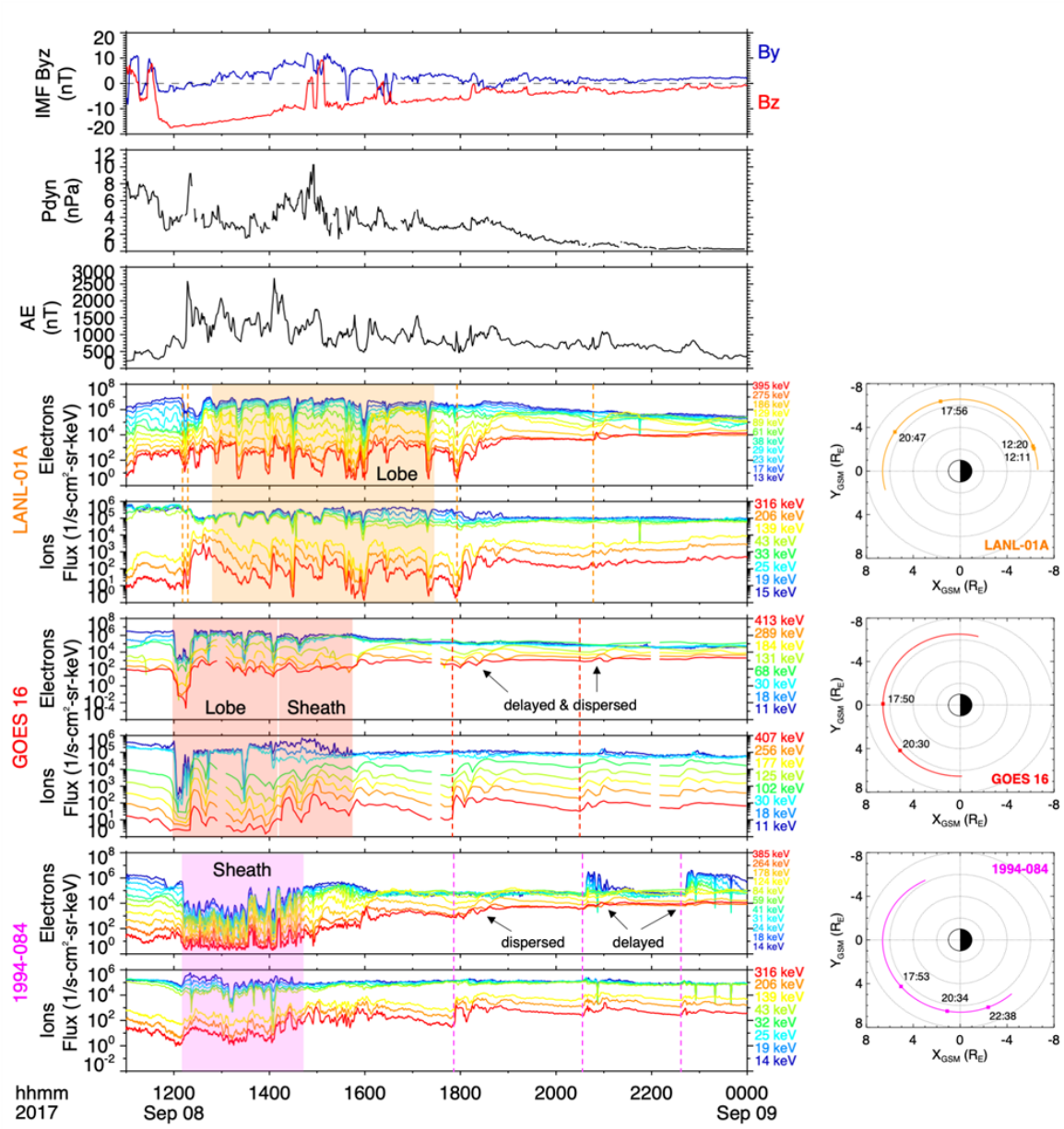

Figure 5. **Observations of particle injections at geo**. Similar to Figure 4, but for the particle injections observed by LANL-97A, LANL-04A and LANL-02A.

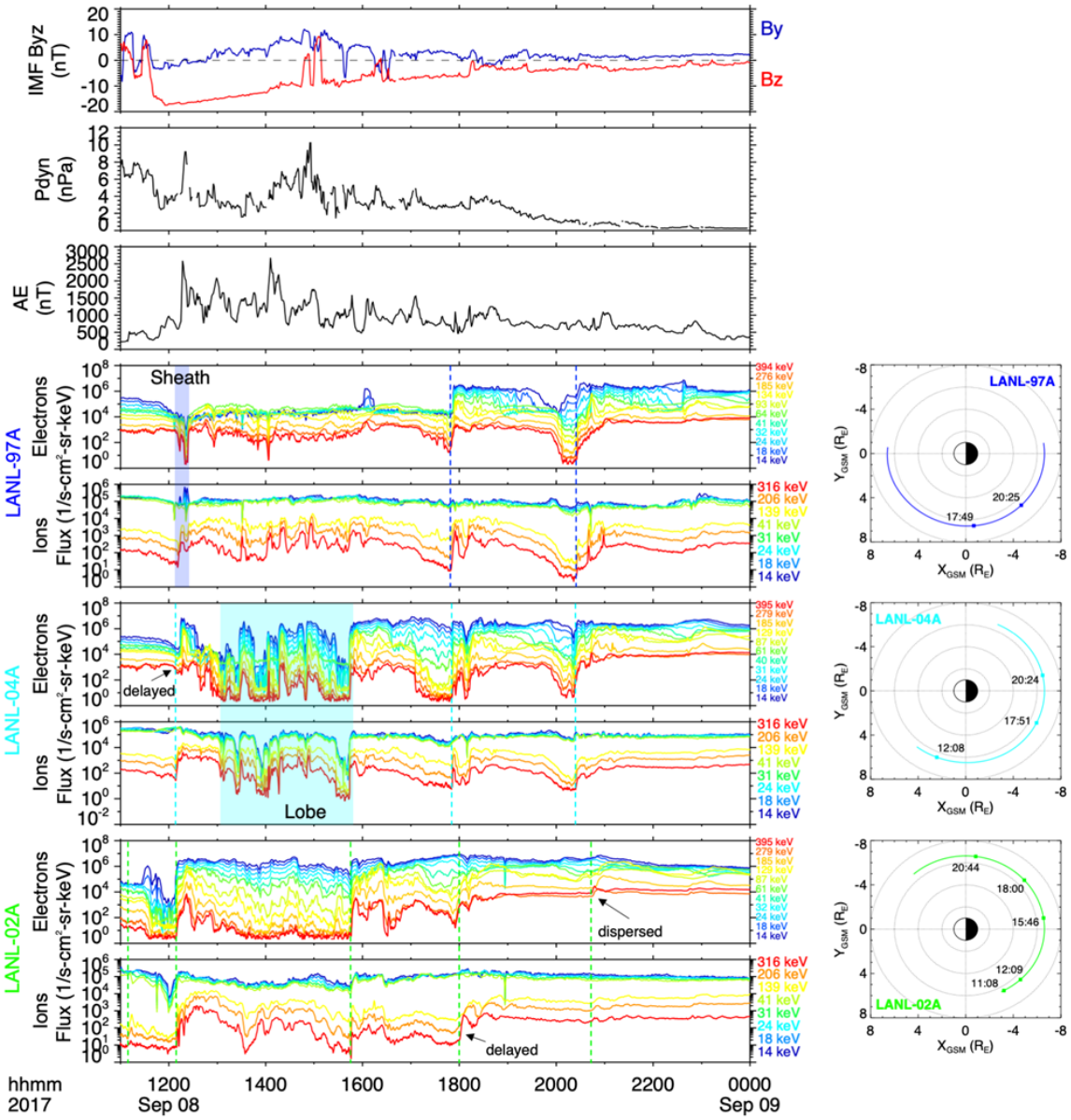

- A first particle injection was observed by LANL-02A at ~1108 UT near dusk local time.
- Subsequent injections were observed in the MLT ~ 17-01 sector around 1210 UT.
- Later, between 15:45 and 23 UT several particle injections were observed at all lcal times.
- Between ~1200 and 1800 UT, there were multiple enhancements of auroral activity, as indicated by the AE index, periods of strong compression, indicated by the peaks in the solar wind dynamic pressure, and strong convection, as indicated by the strong southward Bz component of the interplanetary magnetic field (IMF).
- The particle injections thus appear to be the signatures of substorm activity and/or magnetospheric compression during a period of strong convection.

INNER MAGNETOSPHERIC RESPONSE

H+ fluxes and injections inside geosynchronous orbit

Figure 6. H+ fluxes observed by the twin Van Allen Probes spacecraft over six orbits during the storm.

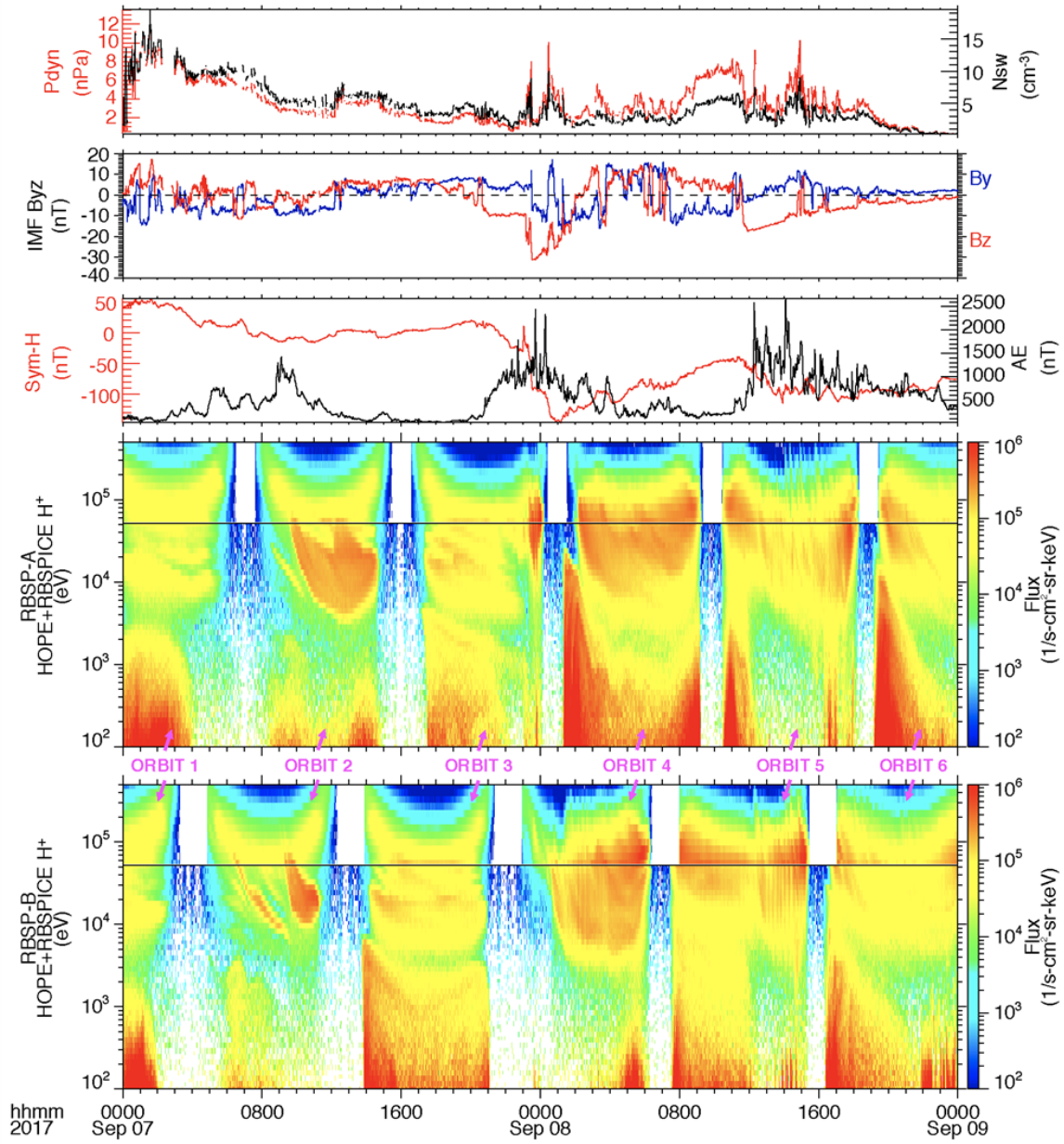

- During the storm, the apogees of both Van Allen Probes (RBSP) satellites were on the dayside near noon local time. RBSP-A followed RBSP-B in a very similar orbital path.
- As the storm developed, both RBSP satellites observed enhanced fluxes of <20 keV H+ near dawn and of >20 keV H+ near dusk.

Figure 7. H+ injections observed by the twin Van Allen Probes spacecraft during orbits 4, 5 and 6.

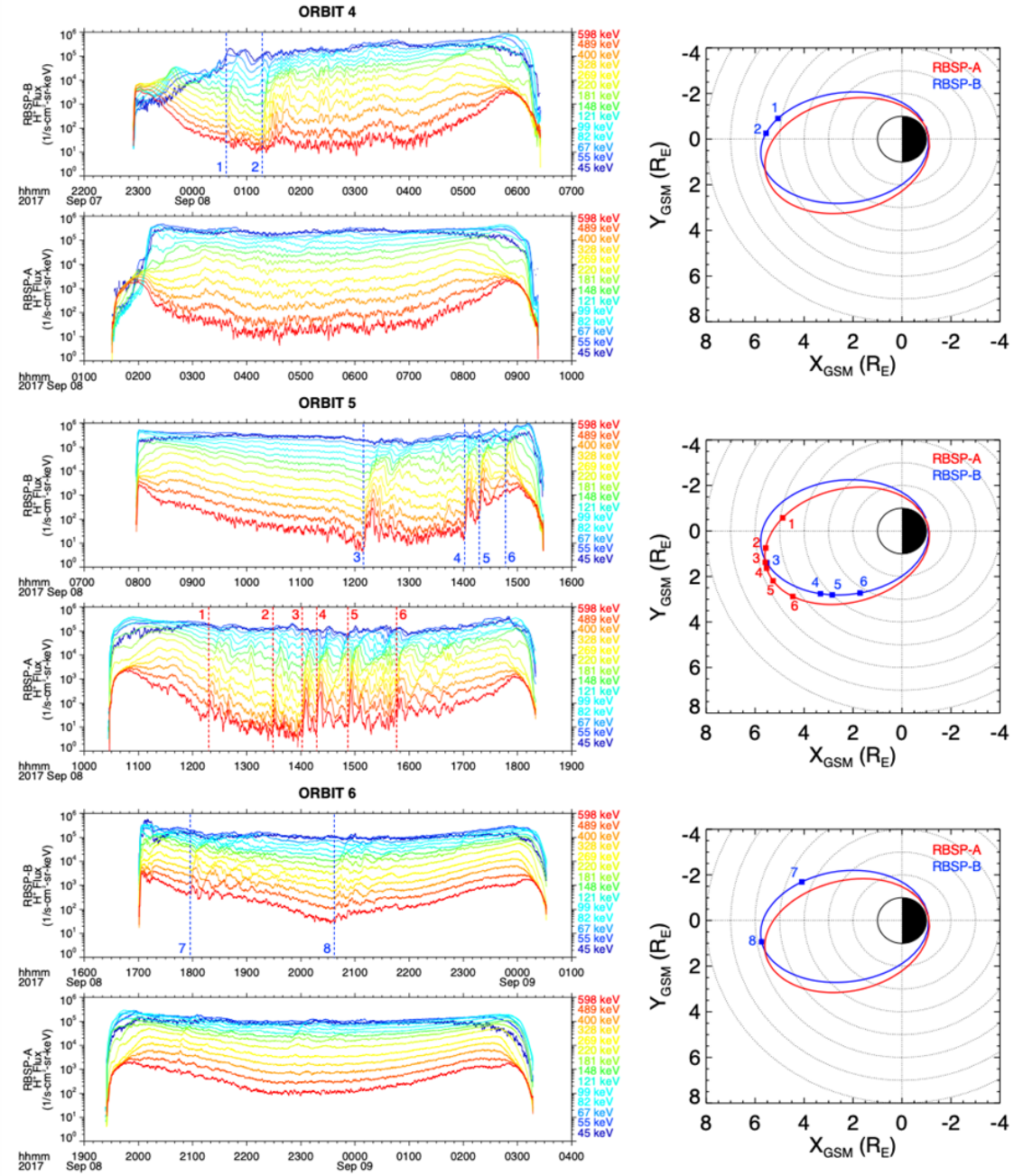

- Between 1200 and 1800 UT, both satellites observed multiple injections, particularly duing Orbit 5.
- The deepest injection signature was observed by probe B at L ~ 3.1.
- The fluxes of the more energetic H+ (~500 keV) were more significantly enhanced by the injections, with flux enhancements of over an order of magntiude.

Cold and warm plasma and wave observations

Figure 8. Observations of strong electric fields and waves in two frequency ranges during orbit 5. From top to bottom, the panels show: the cold electron density from EMFISIS, the H+ and O+ fluxes from HOPE and RBSPICE, the y- and z-components of the vector electric field from EFW, and the Poynting flux in two frequency ranges, a high-frequency (10-180 sec) and a low-frequency (5-15 min) range.

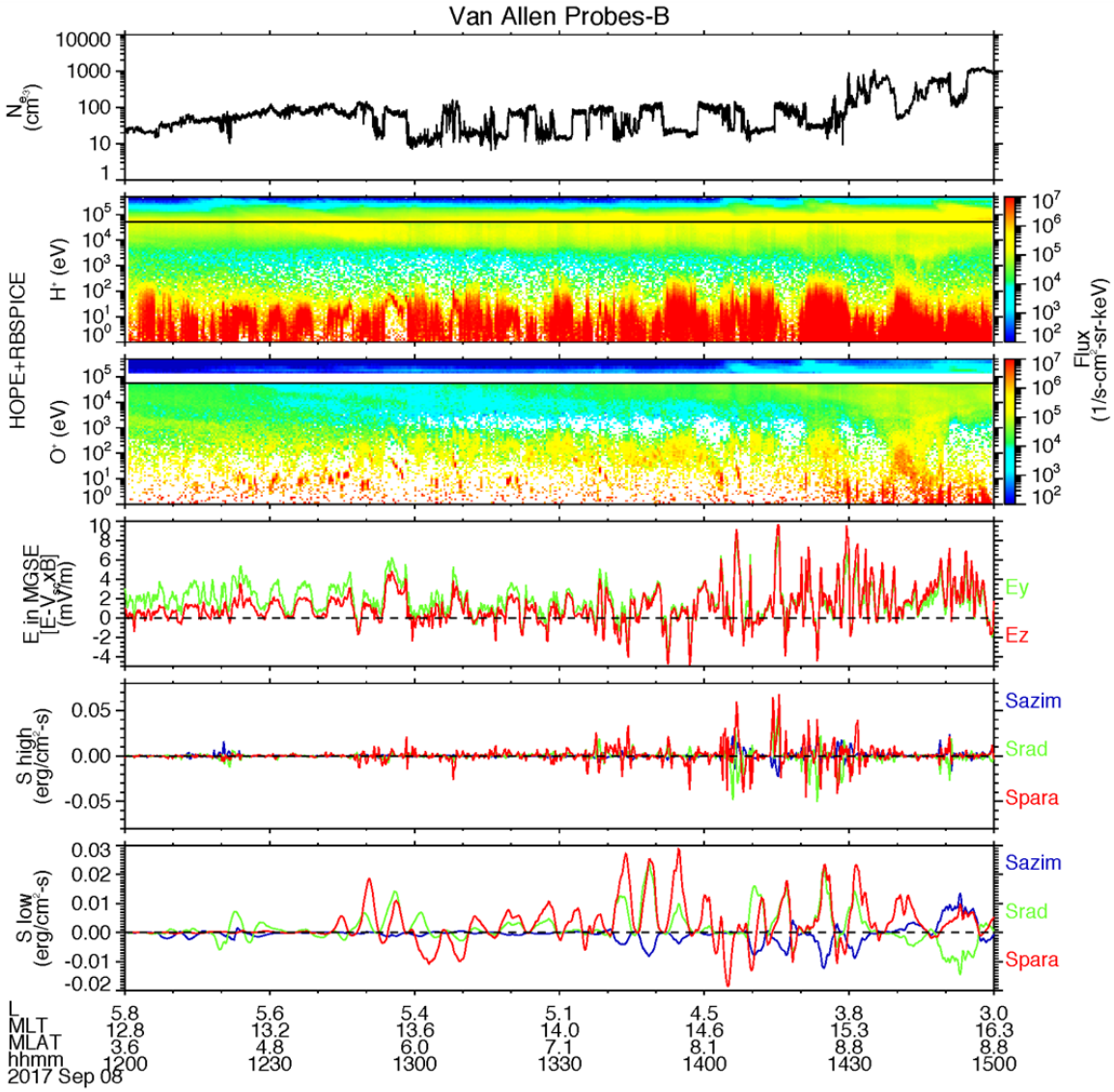

- 5-10 min density dips are observed in correspondence with enhanced ~1-100 eV particle flux.
- Strong electric fields (~8 mV/m) are observed down to L~3.
- Based on the E to B ratio, the high-frequency waves are likely Alfven waves.
- The low-freqency waves exhibit strongly directional Poynting flux and are likely associated with field aligned currents, also based on the E to B ratio.
- The corresponding field aligned Poynting flux in both frequency ranges is ~0.01-0.04 ergs/cm^2-s. A rough estimate, using a scaling of 1/L^3, gives that the Poynting flux intensity mapped to the ionosphere is ~0.9-3.6 ergs/cm^2-s (for context, ~1 erg/cm^2-s corresponds to the threshold for visible aurora).
- What were the effects of these waves on the cold and warm particles?

DATA-MODEL COMPARISON AND CONCLUSIONS

The effect of the boundary conditions in the model

Figure 9. Comparison of H+ fluxes for two CIMI runs with different boundary conditions (BC). The top panel shows H+ fluxes measured by RBSP-A and the bottom two panels show H+ fluxes from two runs with the CIMI model with different BC: one using an empirical model (middle panel) and the other using measurements at geosynchronous orbit (bottom paenel).

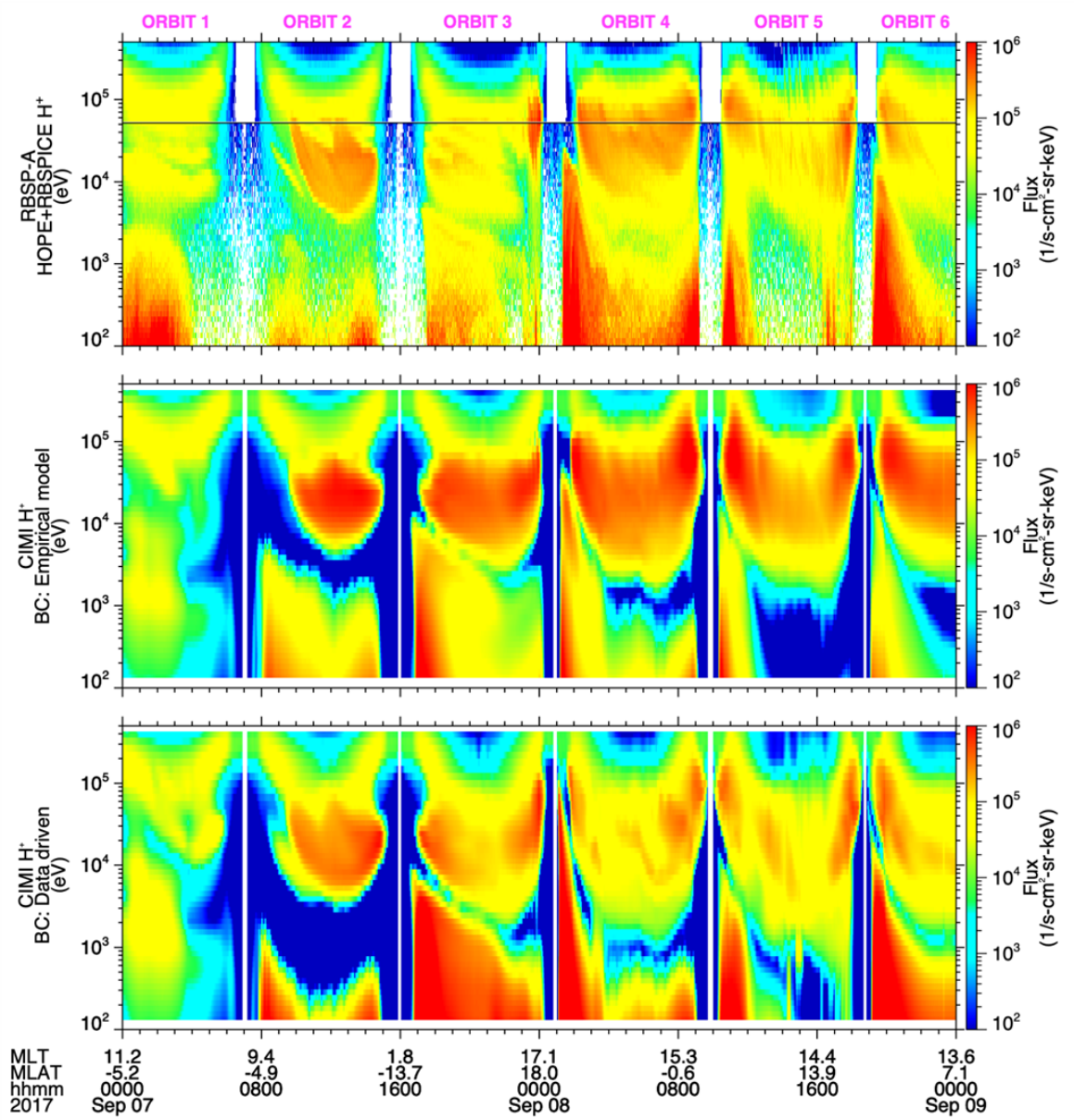

- Whereas the run with BC determined by the empirical model (EM) of Ebihara and Ejiri captures the general dynamics and reproduces the general features of ring current H+ during the storm, the run with data-driven (DD) BC determined from measurements at geo captures much better the flux intensity and the small-scale features.

Figure 10. Comparison of H+ fluxes for two CIMI runs with different boundary conditions (BC) over orbit 5. Similar to Figure 9, the top panel shows the measured H+ fluxes and the two bottom panels the simulated H+ fluxes.

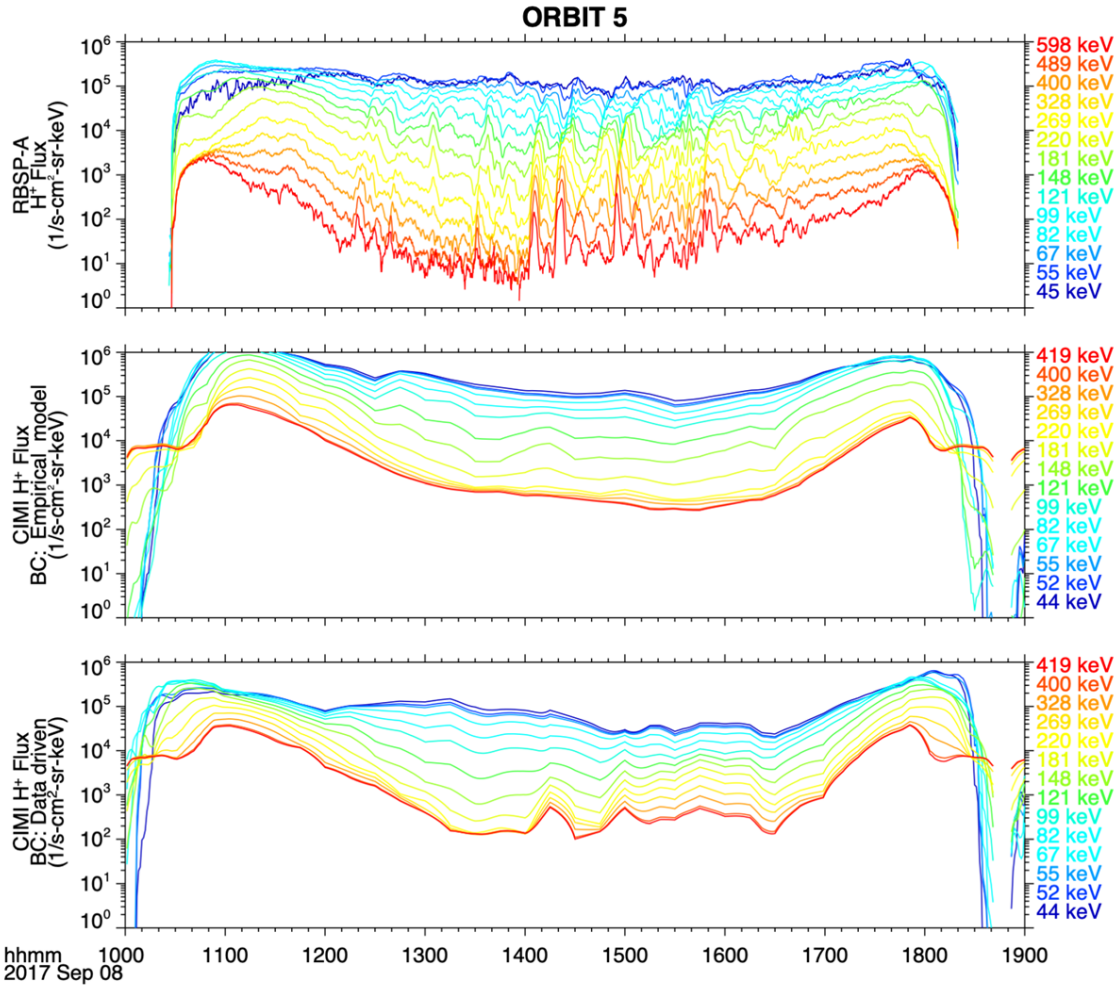

- A close-up look at orbit 5, shows that the run with data-driven BC captures some of the observed injections between 1200 and 1800 UT, whereas the run with empirical BC does not.

- This emphazises the important role of the source population in modeling the ring current.

The effect on the ring current development

Figure 11. Comparison of the total ring current pressure for two CIMI runs with different boundary conditions (BC).

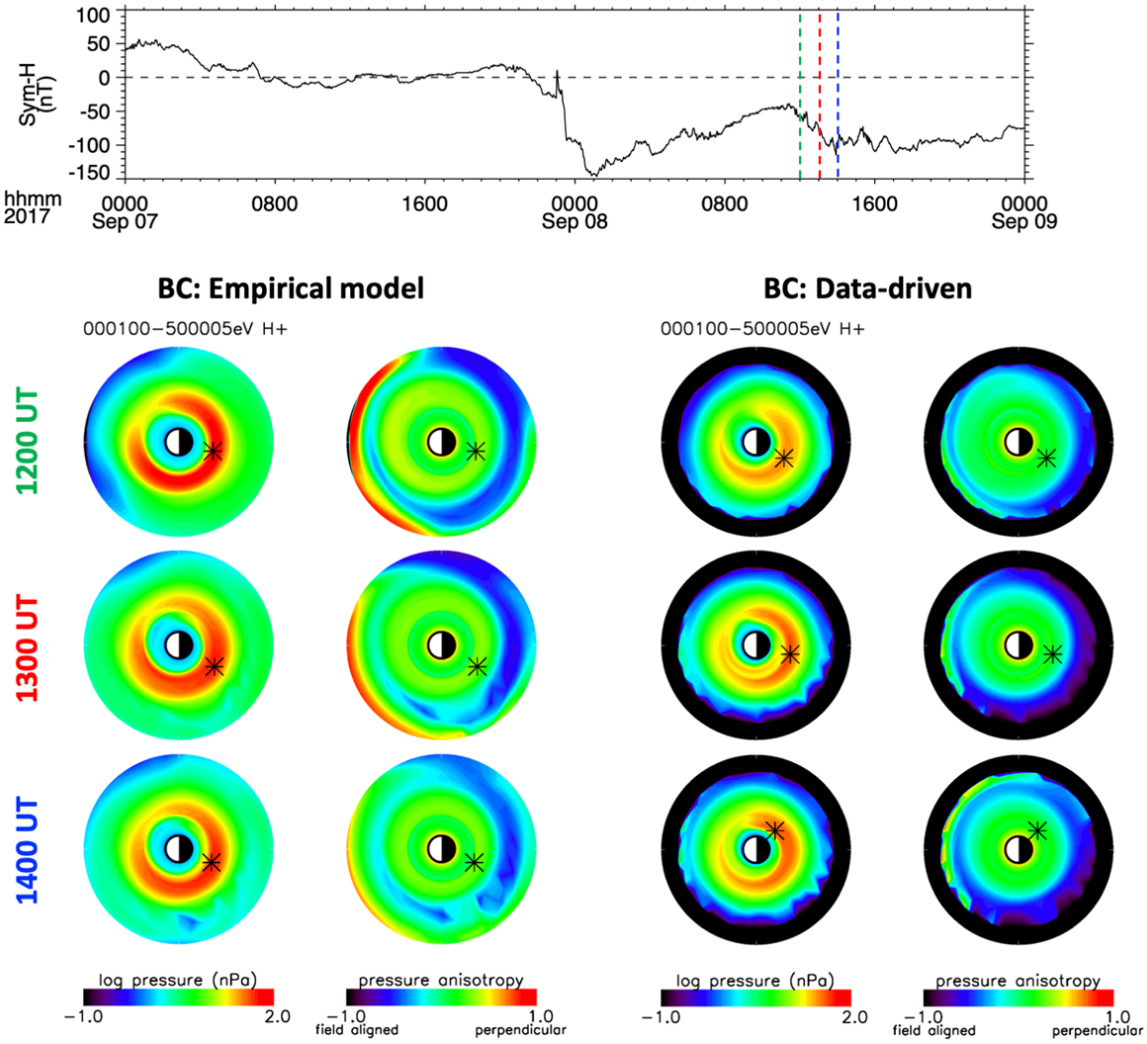

The effects of including the particle distributions observed at GEO as the BC in the model are the following:

- The total ring current pressure is overall lower, but it is higher at the low L shells.
- After particle injections are observed at GEO around 1200 UT on September 8, the ring current pressure exhibits two peaks on the duskside at 1300 UT.
- At 1400 UT, the peak pressure (indicated by the asterisk) shifts to the dawnside, where two peaks in pressure are obsreved.
- The ring current pressure distribution takes longer to become symmetric in local time.

Figure 12. Comparison of the equatorial potential and electric field for two CIMI runs with different boundary conditions (BC).

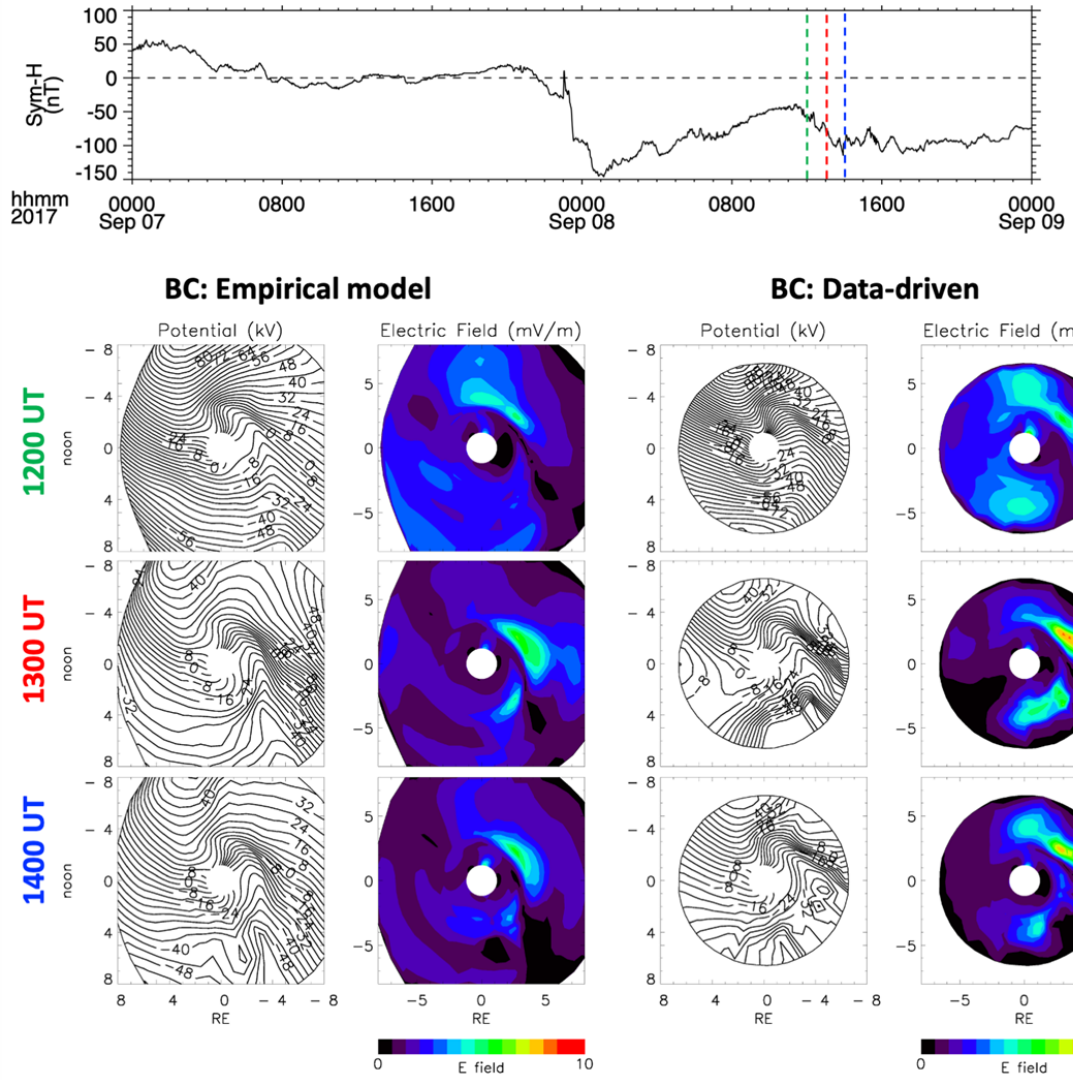

- Particle injections observed at GEO around 1200 UT are associated with the stronger electric field on the nightside over a larger range in L for the run with data-driven BC.
- At 1300 UT the electric field is clearly stronger on both the pre- and post-midnight sectors, but especially toward dawn.
- These strong electric fields are responsible for the deeper access of ring current ions in the run with data-driven BC.
- By 1400 UT, strong electric fields persist in the post-midnight sector, which explains the deep access of ring current ions in this sector and the associated shift in peak pressure toward dawn.

Conclusions

- This storm event is characterized by a severe deformation of the magnetospheric magentic field, evident by the sheath crossings and lobe encounters by satellites at GEO.
- Substorm particle injections over wide local time sectors are observed at GEO and deep in the dayside inner magnetosphere.
- The particle injections are associated with electric field enhancements particularly on the post-midnight sector and are responsible for changing the pressure distribution of the ring current in local time and for prolonging the time over which the ring current is asymmetric.
- The ring current asymmetry and the associated field aligned currents during this event might be partly responsible for the observed strong electric fields and waves, and the severe plasmaspheric erosion (not shown here, but shown in Naomi

Maruyama's poster: /?s=94-12-2E-A7-C4-81-17-4A-67-EB-17-B3-53-FB-66-44 (/?s=94-12-2E-A7-C4-81-17-4A-67-EB-17-B3-53-FB-66-44)).

- The contribution of the particle injections to the ring current pressure still needs to be estimated.

AUTHOR INFORMATION

Cristian Ferradas, Mei-Ching Fok, Naomi Maruyama, Andrew Menz, Michael Henderson, Brian Kress, Sam Califf, and Scott Thaller

ABSTRACT

The event of 8 September 2017 was characterized by the effects of the arrival of two interplanetary coronal mass ejections on September 6th and 7th and a resultant geomagnetic storm. This storm event has been widely studied due to its extreme geo-effectiveness in the global geospace. In the inner magnetosphere, the effects included a distinct intensification of the ring current and a severely eroded plasmasphere. However, little attention has been paid to the role that the observed substorm injections played on the storm-time ring current. Starting at 1209 UT on September 8th, multiple substorm onsets occurred spreading over a wide magnetic local time range on the dawn side. Multiple substorm injections were observed simultaneously at geosynchronous orbit by the Los Alamos National Laboratory satellites and the Geostationary Operational Environmental Satellites, and by both the Exploration of energization and Radiation in Geospace/Arase and the Van Allen Probes missions deep in the inner magnetosphere. Subsequent buildup of the ring current was observed. In this study, we will investigate the role of the substorm injections on the extreme ring current response by numerical simulations with the physics-based Comprehensive Inner Magnetosphere-Ionosphere model using the geosynchronous data as boundary conditions to the model. Since the ring current has a strong influence on the inner magnetospheric dynamics, we also consider its impacts on the dynamics of the electric field and the plasmasphere. Furthermore, this study addresses the critical need to include substorms in evaluating the geo-effectiveness of geomagnetic storms.